by E. S. Cooper

Disk file access-time constraints imposed by magnetic air-bearing compliance

Use is commonly made of coil voltages which produce maximum acceleration and deceleration to wrest the fastest access performance from the actuator of a disk file. Alternatively, equivalent performance is easily obtained with less control optimality by simply increasing the coil voltage. A limit to greater coil voltage, however, arises from the need to avoid harmful effects when the servo loses control of the actuator, the actuator slams into its crash stop, and the crash force stresses the magnetic head air bearing. Magnetic head air-bearing compliance, therefore, is one of three fundamental constraints that limit the access-time performance of an actuator. To obtain

[©]Copyright 1990 by International Business Machines Corporation. Copying in printed form for private use is permitted without payment of royalty provided that (1) each reproduction is done without alteration and (2) the *Journal* reference and IBM copyright notice are included on the first page. The title and abstract, but no other portions, of this paper may be copied or distributed royalty free without further permission by computer-based and other information-service systems. Permission to *republish* any other portion of this paper must be obtained from the Editor.

improved access-time performance from a disk file, the following should be optimized: the airbearing slider, the actuator crash stop, and the actuator mechanical time constant. This paper presents relevant design considerations.

Introduction

Many competing design considerations combine to establish the seek capability of a high-performance disk file. In an effort to achieve faster actuator access times, three fundamental design constraints of the magnetic head/disk assembly (HDA) of the disk file are encountered: (1) the power-dissipation capability of the actuator coil, (2) the mechanical dynamics of the actuator and baseplate, and (3) the maximum deceleration forces of the crash stops as limited by airbearing compliance.

The first constraint, that of power dissipation, derives from an inverse fourth-power relationship between access time and actuator coil power. Shortening the access time of a disk file to half of its original value, for example, produces a sixteenfold increase in dissipation. Degrading aspects of retuator power dissipation are the generation of temperature gradients within the HDA which contribute to track misregistration. Additionally, excessive coil temperatures destroy coil bonding material, cause deterioration of the mechanical dynamic properties of the coil, and degrade actuator seek performance by worsening the global tolerances accommodated by the access servo deceleration trajectory. Problems of power dissipation are well known, and literature [1] exists that prescribes minimum power design formulations for the actuator coil and the control trajectory.

Actuator and baseplate mechanical dynamics are the second constraint to improved HDA access time. Actuator dynamics limit access servo bandwidth and restrain seek-time performance for short distances. Baseplate dynamics, which are excited by actuator reaction forces, prolong seek-settling properties of the HDA. Both actuator and baseplate dynamics are considerations in the minimization of track misregistration (TMR) due to nonrepeatable runout (NRRO); actuator dynamics limit track-regulating bandwidth, and baseplate resonances must not coincide with spindle-bearing frequencies. Literature exists that addresses the track-regulating [2–4] and seek [5, 6] problems.

The air-bearing compliance of the magnetic head is the third constraint and is the subject of this paper. Airbearing compliance is defined as the permissible reduction of the magnetic head/disk spacing from its nominal value before the air bearing fails. No literature exists that relates the access performance of a disk file to its magnetic head air-bearing compliance. Magnetic head/disk interface papers typically relate either airbearing dynamics [7] or air-bearing measurement techniques [8, 9]. Alternatively, access-time-related papers [10] associate actuator performance with actuator magnetic and coil-design parameters, but neglect the implications of air-bearing compliance. One paper, by Tokuyama et al. [11], formulates reduction of magnetic head slider flying height to slider acceleration forces, but with no relationship to actuator access time.

If a switchable voltage source is applied to an actuator coil, and if mechanical dynamics are ignored, arbitrarily improved access time through use of greater acceleration and deceleration may be achieved by applying a greater coil-control voltage. As coil voltage is increased, however, two constraints are encountered. These constraints are the maximum permissible power dissipation of the actuator, which rapidly increases as the inverse fourth power of access time [1], and the maximum allowable impact velocity to the actuator crash stops.

The crash-stop constraint ensues from a requirement to guarantee minimum air-bearing spacing between the magnetic head slider and the magnetic media. The

greatest stress to air-bearing spacing is encountered when the access servo loses control of the actuator and the actuator slams into its crash stop with a very large resultant radial deceleration force. However, properties of the magnetic head slider, its suspension, and the air bearing establish a maximum permissible deceleration rate that is usually several hundred times that of gravity. This maximum permissible deceleration rate, coupled with crash-stop design and HDA compression allocation, in turn constrains the actuator's maximum radial impact velocity. Maximum impact velocity then limits the maximum applied coil-control voltage and produces a limit on actuator seek acceleration and deceleration rates. The limit on actuator rates of acceleration and deceleration produces a bound on achievable access time. The design problem, therefore, is to achieve minimum access time, subject to a lower air-bearing-spacing limit that is encountered during the maximum velocity impact of the actuator to the crash stop.

The first section of this paper considers the angular moments acting upon the magnetic head slider and relates the permissible air-bearing compliance of the slider to an induced radial deceleration constraint. Since the greatest deceleration occurs during the crash process, the design of the crash stops is considered next, in the second section. A comparison is made between the performance of the usual idealized constant-spring-rate crash stop and the optimal constant-force crash stop. The third section joins the air-bearing constraint and the crash-stop design to actuator access time, and it is found that actuators with fast mechanical time constants provide superior performance. Finally, a prescription for the design of actuators to achieve fast mechanical time constants is offered.

Magnetic head slider and air bearing

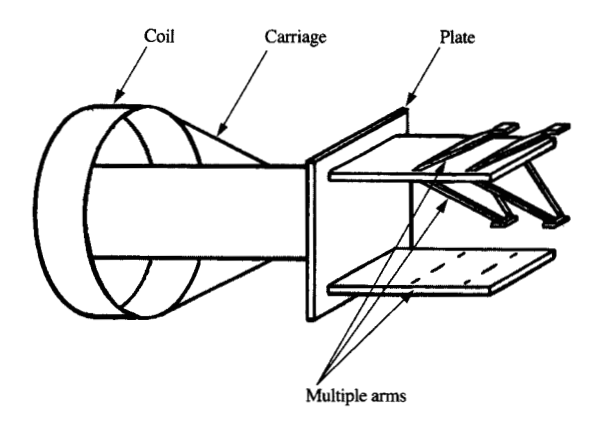
Consider the actuator with its magnetic head, slider, and suspension, as shown in Figure 1. The slider radial deceleration force acting through moment arm S induces an applied moment on the slider about its axis of rotation of

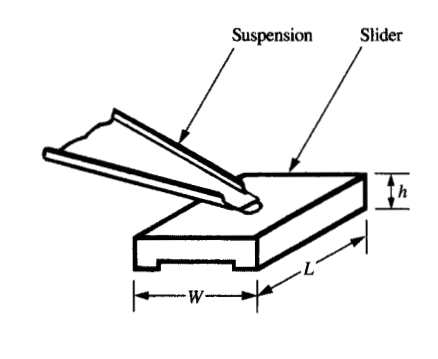
$$M_{\rm D} = WLhS\ddot{x}\delta,\tag{1}$$

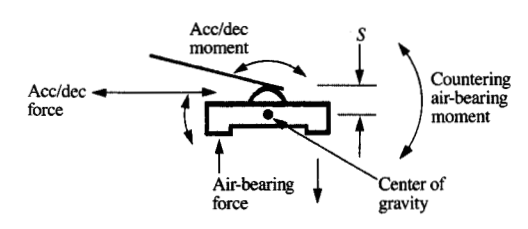
where W is the slider width measured radially to disk axis, L is the tangentially measured slider length, h is the slider height, S is the moment distance between the center of gravity of the slider and its applied radial deceleration force, \ddot{x} is the radial acceleration of the slider, and δ is its material density.

Opposing the moment produced by radial acceleration/deceleration forces are the respective moments of each air-bearing surface. The two air-bearing surfaces provide a countering moment $M_{\rm ab}$ of

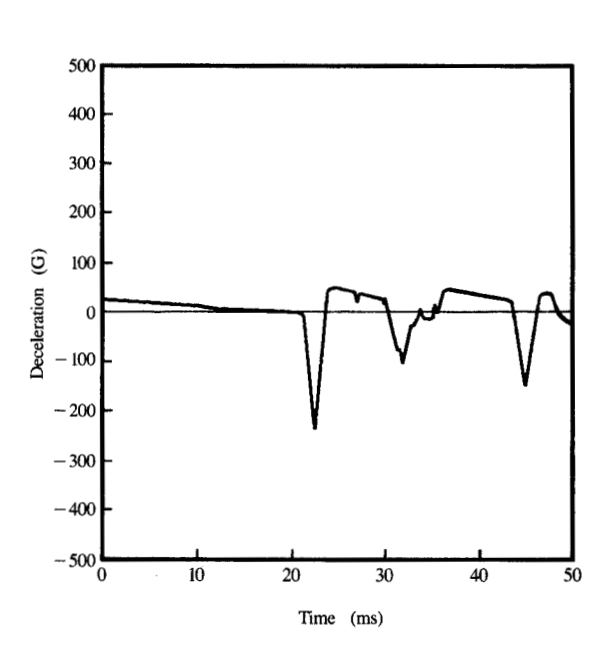
669







Actuator with magnetic head, slider, and suspension.



Element.

Typical time response of crash process

$$M_{\rm ab} = 2\left(\frac{W}{2} k_{\rm s} Z \zeta W L\right) = W^2 L k_{\rm s} \zeta Z,\tag{2}$$

where $k_{\rm S}$ is the linearized air-bearing spring constant per unit of air-bearing surface, ζ is the scaling of air-bearing surface area to slider width W and length L, and Z is the air-bearing displacement measured normal to the disk surface. Note that $k_{\rm S}$ is a second-order function of radial velocity. For pedagogical reasons, $k_{\rm S}$ is assumed constant. The simulated/measured roll stiffness of the air bearing permits calculation of $k_{\rm S}$ and ζ .

Shown in Figure 2 is a typical time response of the crash process in which a constant voltage is applied to the actuator during its portrayed 50-ms duration. The actuator traverses its full stroke distance in approximately 22 ms and repeatedly collides with and recoils from the same crash stop. It is seen that the maximum impact deceleration is 250 G, where G is the usual gravitational acceleration of 9.8 m/s².

Note that air-bearing dynamics, which have natural resonance frequencies in the 20–30-kHz range, produce only a small modulation upon the portrayed impact deceleration force. In the following analysis, therefore, a simplification is made to neglect the contributions of high-frequency air-bearing dynamics. By equating radial deceleration force moment to countering air-bearing

moment, the steady-state air-bearing compliance may be expressed as a function of slider radial deceleration, \ddot{x} :

$$M_{\rm D} = M_{\rm ab},$$

$$WLhS\ddot{x}\delta = W^2Lk_{\rm S}\zeta Z,$$

$$\ddot{x} = \frac{Wk_{\rm S}\zeta Z}{hS\delta}.$$
(3)

This suggests that effects of radial deceleration on airbearing compliance can be minimized with large slider width, reduced material density, reduced slider height, reduced distance between slider center of gravity and flexure attachment, and large air-bearing preload force (which increases the spring constant per unit surface area). A double-height slider, in which h and S are each made double their initial value, for example, should provide a fourfold degradation or decrease in permissible radial deceleration rate.

Crash-stop design

The crash-stop design originates from the satisfying of two criteria. The first criterion is to maintain minimum air-bearing spacing during the actuator crash process. Violation of the minimal spacing criterion during crash-stop impact increases the probability of catastrophic failure of the air bearing and irrevocable loss of user data. The second criterion is to accomplish the first, but with minimal crash-stop compression. Crash-stop compression consumes disk area that otherwise amortizes total product cost and provides lower product cost per data storage gigabyte. Commonly, up to 20 percent of available disk radius (10 percent at each travel extremity) is expended by crash-stop compression which might otherwise be used for data storage.

Satisfaction of the two criteria is difficult because of the range of temperatures encountered in the HDA. Commonly, the crash stop is composed of some rubberlike material whose resilience properties diminish drastically with increased temperature. The reduced resilience makes it easy to satisfy the first criterion, but makes the second less tractable. Lower temperatures induce a corresponding reversal of difficulty in meeting the criteria.

More complicated crash-stop designs which are less temperature-sensitive may employ some form of metallic spring. A metallic spring has a spring rate that is virtually independent of temperature. Additionally, it permits the use of preload techniques that make deceleration force approximately constant with displacement. Deceleration-rate criteria are thereby satisfied with a preload spring design, but with reduced compression distance. A difficulty with this design is the prevention of sharp impact forces as actuator and crash stop make contact.

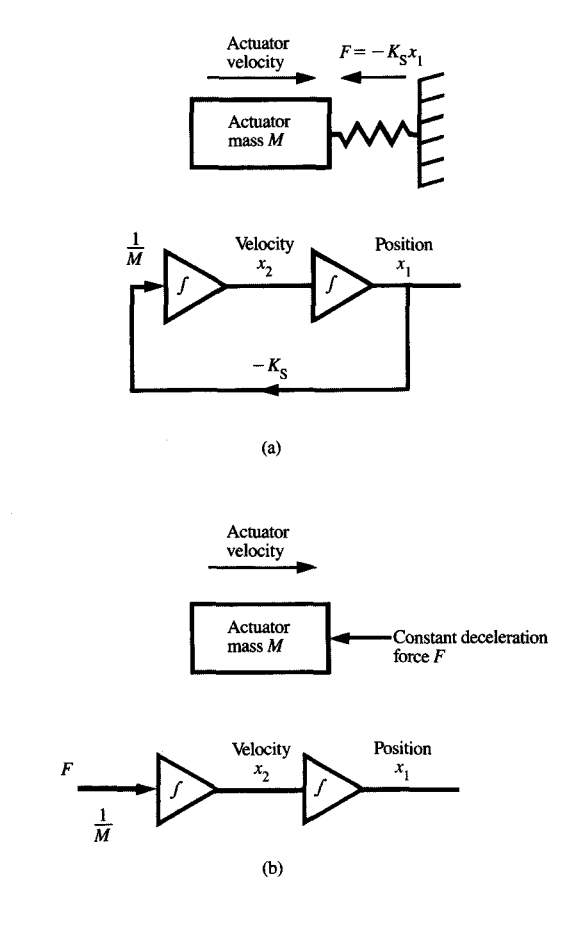
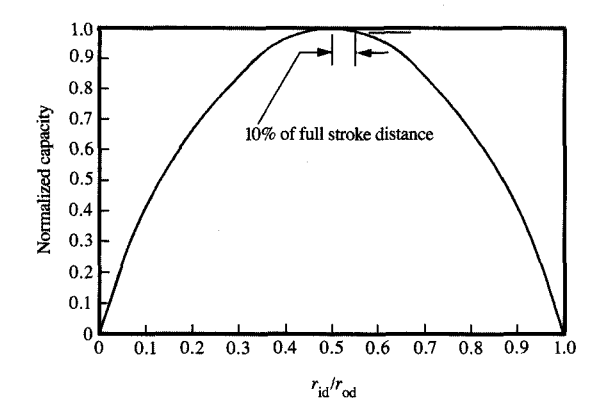


Figure 8

(a) State diagram of actuator impacting, with crash-stop force modeled as an ideal spring force. (b) State diagram of actuator impacting with a crash-stop force modeled as a constant deceleration force.

The maximum possible impact velocity can be calculated from the maximum deceleration rate of the air bearing, \ddot{x}_{max} , and minimum crash-stop-compression distance. Consider, therefore, two crash-stop designs: one is the simple spring, which approximates a rubber crash stop; the other is the optimal preloaded metal spring that provides constant deceleration force and produces minimum possible crash-stop-compression distance.

Figure 3(a) shows the state diagram of the approximated rubber-crash-stop force upon a double-integrator actuator. If x_i and x_2 are actuator position and velocity, respectively, their state equations can be written as



Normalized disk capacity for constant recording frequency.

$$\begin{bmatrix} \dot{x}_1(t) \\ \dot{x}_2(t) \end{bmatrix} = \begin{bmatrix} 0 & 1 \\ -K_S & 0 \\ \hline M & 0 \end{bmatrix} \begin{bmatrix} x_1(t) \\ x_2(t) \end{bmatrix}, \tag{4}$$

with transient response to initial conditions $x_1(0)$, $x_2(0)$,

$$\begin{bmatrix} x_1(t) \\ x_2(t) \end{bmatrix} = \begin{bmatrix} \cos(\omega_n t) & \frac{1}{\omega_n} \sin(\omega_n t) \\ -\sin(\omega_n t) & \cos(\omega_n t) \end{bmatrix} \begin{bmatrix} x_1(0) \\ x_2(0) \end{bmatrix}, \tag{5}$$

where

$$\omega_n = \sqrt{\frac{K_{\rm S}}{M}}$$

By differentiating the time solution for velocity to obtain deceleration and equating its peak deceleration at $x_{1\text{max}}$ to \ddot{x} , the maximum impact velocity $x_2(0)$ may be found:

$$x_2(0) = \sqrt{\bar{x}x_{1\text{max}}}, \tag{6}$$

where $x_{1\text{max}} = x_1(t)$ when $x_2(t) = 0$.

Figure 3(b) shows the state diagram of the optimal crash stop in which a constant deceleration force F is applied. The resulting state differential equation is

$$\begin{bmatrix} \dot{x}_1(t) \\ \dot{x}_2(t) \end{bmatrix} = \begin{bmatrix} 0 & 1 \\ 0 & 0 \end{bmatrix} \begin{bmatrix} x_1(t) \\ x_2(t) \end{bmatrix} - \begin{bmatrix} 0 \\ \frac{1}{M} \end{bmatrix} F, \tag{7}$$

with transient response

$$\begin{bmatrix} x_1(t) \\ x_2(t) \end{bmatrix} = \begin{bmatrix} 1 & t \\ 0 & 1 \end{bmatrix} \begin{bmatrix} x_1(0) \\ x_2(0) \end{bmatrix} - \begin{bmatrix} \frac{t^2}{2} \\ t \end{bmatrix} \frac{F}{M}, \tag{8}$$

By solving for the deceleration time required to reduce initial impact velocity $x_2(0)$ to zero, the maximum impact velocity as a function of traverse distance is found to be

$$x_2(0) = \sqrt{2x_{1\text{max}}}\dot{x} \,. \tag{9}$$

Comparison of Equation (9) with Equation (6) shows that the optimal crash stop, as shown in Figure 3(b), provides a $\sqrt{2}$ improvement in maximum impact velocity. Conversely, for identical impact velocities the ideal crash stop requires only half the compression distance of the rubber crash stop. Inclusion of the temperature dependence of the rubber crash stop makes the comparison even more pronounced. Practical preload spring crash stops, on the other hand, only approach the performance of the ideal crash stop.

Up to 20 percent of available disk radius may be employed for crash-stop compression. For conventional, inner-to-outer-radii, constant-frequency disk recording, however, only the outer crash-stop compression distance appreciably degrades product cost per gigabyte. Constant-frequency disk recording is the usual scheme, in which the linear bit density of the disk is inversely proportional to its radius in order to maintain a constant frequency of magnetic flux reversals per second. The disk capacity for constant recording frequency is

$$C = TPM(r_{od} - r_{id})2\pi r_{id}BPM, \tag{10}$$

where C is the disk capacity, TPM is the number of tracks per meter, BPM is the recording density in bits per meter at $r_{\rm id}$, $r_{\rm id}$ is the data band inner radius, and $r_{\rm od}$ is the data band outer radius.

A plot of constant-frequency disk capacity as a function of the ratio between inner and outer radii is shown in **Figure 4**. The radius ratio maximizing disk capacity requires $r_{\rm od}=2r_{\rm id}$, but it is easily seen that deviation from optimality at the inner radius, such as incurred by 10 percent of full stroke compression distance, produces an imperceptible one percent loss of disk capacity. Few high-performance disk file designs achieve true capacity optimality, but rather exchange a small capacity loss for significant benefits in disk dynamics and actuator power.

On the other hand, for constant linear bit density storage architectures, as approximated by data-banded designs, the loss of capacity due to inner crash-stop compliance enters entirely into a loss of disk capacity.

Crash-stop component cost ranges from 1 to 20 dollars, subject to crash-stop complexity; a high-performance HDA and its supporting electronics may cost upwards of one thousand dollars. Since combined inner and outer crash-stop compression may consume up to 20 percent of available disk area, use of an improved crash stop provides considerable leverage for reducing total product cost per storage gigabyte.

Slider air bearing, crash stop, and average access time

Use of a small magnetic head slider and an optimal crash stop, as defined in the previous sections, permits the use of increased actuator crash-stop impact velocity. We next consider how to relate the increased impact velocity to improvement in actuator move time (actuator move time + settle time = actuator access time). Improvement of the average move time that ensues from an increased permissible impact velocity is not straightforward, but depends upon properties of the actuator and the probability density function relating to the occurrence of specific seek lengths.

Consider, therefore, the idealized double-integrator actuator of Figure 5 with the state differential equation,

$$\begin{bmatrix} \dot{x}_1(t) \\ \dot{x}_2(t) \end{bmatrix} = \begin{bmatrix} 0 & 1 \\ 0 & -\beta \end{bmatrix} \begin{bmatrix} x_1(t) \\ x_2(t) \end{bmatrix} + \begin{bmatrix} 0 \\ \alpha \end{bmatrix} V_{\text{coil}}, \tag{11}$$

where

$$\alpha = \frac{K_{\rm f}}{MR_{\rm coil}}$$

$$\beta = \frac{K_{\rm f}^2}{MR_{\rm coil}}$$
 linear actuator,

in which K_f is linear motor force constant, M is actuator moving mass, and R_{coil} is motor coil resistance, and

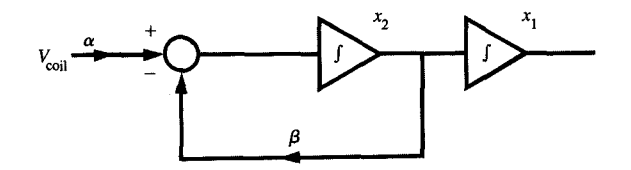
$$\alpha = \frac{K_{t}}{JR_{coil}}$$

$$\beta = \frac{K_{t}^{2}}{JR_{coil}}$$
rotary actuator,

in which K_t is the rotary motor torque constant, J is the rotary inertia of the actuator, and R_{coil} is the motor coil resistance. Note that K_t and K_t , which are idealized constants, are actually nonlinear, time-varying functions of position and current.

The acceleration constant α and the reciprocal of the mechanical time constant ($\beta \equiv 1/\tau$) completely characterize the transient response of the actuator to an applied coil voltage. At the initial application of coil voltage, the actuator accelerates at the rate of $\alpha V_{\rm coil}$. As the velocity of the actuator increases, however, induced back emf within the actuator diminishes the rate of acceleration until a final velocity of $\alpha V_{\rm coil}/\beta$ is asymptotically obtained. The resultant velocity trajectory depends exponentially on τ .

Clearly, a decrease in β , as obtained for example by reducing motor back emf while keeping $\alpha V_{\rm coil}$ constant, provides improved seek performance. Of interest, however, are the resulting detrimental effects on crash-stop velocity, and alternative means for obtaining



	Linear	Rotary
α	$\frac{K_{\rm f}}{MR_{\rm coil}}$	$\frac{K_{\rm t}}{JR_{\rm coil}}$
β	$\frac{K_{\rm f}^2}{MR_{\rm coil}}$	$\frac{K_{\rm t}^2}{JR_{\rm coil}}$

Figure 5

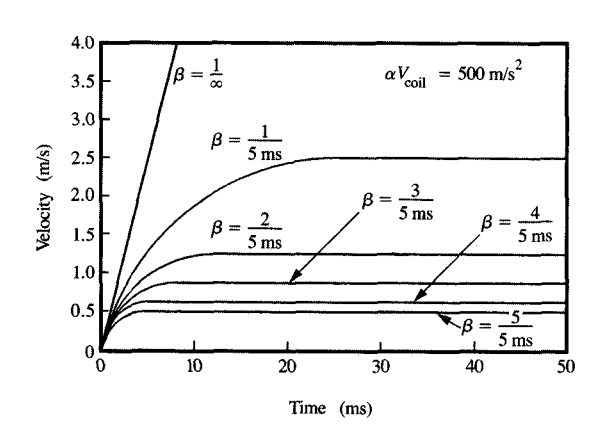
State diagram of idealized linear or rotary actuator, showing back emf and applied coil voltage. The table relates linear and rotary actuator properties to input and feedback elements α and β .

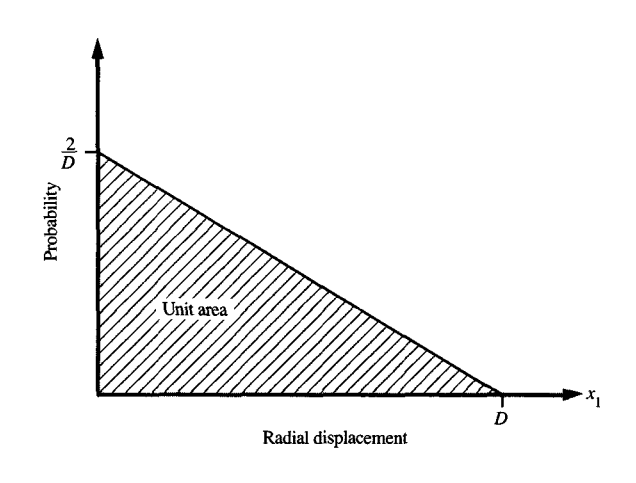
identical move time, but with reduced crash-stop impact velocity.

A series of average move-time and impact-velocity curves are therefore calculated for incremental values of acceleration/control voltage product, $\alpha V_{\rm coil}$, and β . These curves are found by using the transient response of each combination of $\alpha V_{\rm coil}$ and β to calculate times for various seek lengths for a full stroke distance of 25.4 millimeters. Examples of time responses for systems with mechanical time constants of ∞ , 5, 2.5, 1.66, 1.25, 1.0 ms and acceleration/control voltage product $\alpha V_{\rm coil} = 500 \text{ m/s}^2$ are shown in Figure 6. Average move time is computed by weighting the time of each seek length by its respective probability of occurrence, which is shown in Figure 7, and is the usual function favoring occurrences of short seeks.

The resultant move-time and impact-velocity curves are shown in **Figures 8** and **9**, respectively. In Figure 8, the average move time is shown versus control product $\alpha V_{\rm coil}$ for different values of β . It is seen that a decreased value of β yields improved move time. In Figure 9, the impact velocity is shown versus the same control product $\alpha V_{\rm coil}$ for different values of β . It is seen that increased mechanical time constants produce greater impact velocity. There is a conflict, therefore, as might be intuitively expected, between improved move time and reduced crash-stop velocity.

A clear perspective of the compromise between move time and impact velocity emerges if the results of Figures

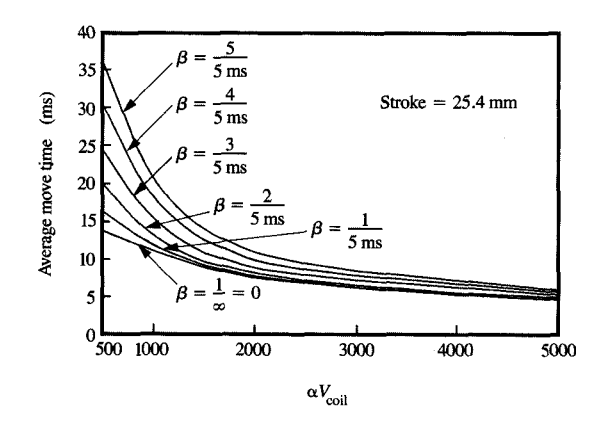




Calculated velocity response of actuators with various mechanical time constants to an applied coil voltage that produces identical initial accelerations.

Figure 7

Probability density function relating the probability of occurrence of specific seek lengths as a function of radial displacement. D is the full stroke distance.



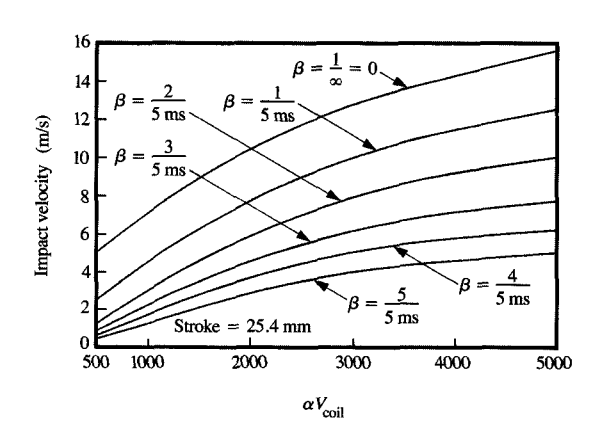


Figure 8

Calculated average move time versus control product $\alpha V_{\rm coil}$, at different values of mechanical time constant $1/\beta$.

Figure 9

Calculated impact velocity versus control product, at different values of mechanical time constant $1/\beta$.

8 and 9 are plotted against each other, as seen in Figure 10. Figure 10 shows that move time is minimized for any impact velocity constraint by designing the actuator to have a faster mechanical time constant. Figure 8, moreover, shows that a faster mechanical time constant alone is not sufficient to achieve faster access time, but additionally, a corresponding increase in control product $\alpha V_{\rm coil}$ is needed.

Figure 10 is useful for determining changes in move time that are achievable by improvements in magnetic head-slider and crash-stop designs. If, for example, the double-height slider (described earlier) that provides a fourfold degradation in radial deceleration were incorporated into the HDA design, then from Equation (6) or (9) it follows that there should be a twofold decrease in permissible impact velocity. Figure 10 shows

that halving permissible impact velocity requires a doubling of the actuator move time, almost independently of its mechanical time constant. For an infinitely long mechanical time constant, for example, an impact velocity of 15.8 m/s warrants a 4.4-ms move time. Halving the impact velocity to 7.9 m/s should permit a 9.6-ms move time, or approximately a doubling of actuator move time.

Similarly, substitution of the optimal crash stop for the rubber crash stop should produce a $\sqrt{2}$ improvement of permissible impact velocity and permit an increase of $\alpha V_{\rm coil}$ that should yield a $1/\sqrt{2}$ reduction of average move time.

Implications for actuator design

In this section we incorporate the design goal of a reduced mechanical time constant into physical actuator design. Both linear and rotary designs are discussed.

• Linear actuator

Consider a linear coil of an actuator as a formed current sheet of fixed dimension of length ℓ , width W, and height h, immersed in an orthogonal magnetic field of intensity B. The N coil turns, each of length ℓ , may be seen as a partitioning of current sheet cross-sectional area into N subareas, as shown in Figure 11. The total mass M of the actuator is assumed to consist of coil mass M_c and the remaining actuator mass M_a . The force factor, coil resistance, and mass of the linear actuator are defined as

$$K_{\rm f} = \gamma B \ell N, \tag{12}$$

$$R_{\text{coil}} = \frac{\ell^2 N^2}{\sigma V},\tag{13}$$

$$M = M_a + M_c = M_a + DV, \tag{14}$$

where D is coil material density, γ is the fractional utilization of coil turn length ℓ by magnetic field B, σ is material conductivity, and $V = \ell W$ is coil volume.

The acceleration constant and the mechanical time constant reciprocal for the system shown in Figure 5 are given by

$$\alpha = \frac{K_{\rm f}}{MR_{\rm coil}} = \frac{\gamma B \ell N}{(M_{\rm c} + M_{\rm a}) \frac{\ell^2 N^2}{\alpha V}}$$

$$= \frac{\sigma V \gamma B}{(DV + M_a)\ell N} = \frac{\sigma W \gamma B}{(DV + M_a)N}.$$
 (15)

$$\beta = \frac{1}{\tau} = \frac{K_{\rm f}^2}{MR_{\rm coil}}$$

$$= \frac{(\gamma B \ell N)^2}{(M_c + M_a) \frac{\ell^2 N^2}{\sigma V}} = \frac{\sigma V \gamma^2 B^2}{(DV + M_a)}.$$
 (16)

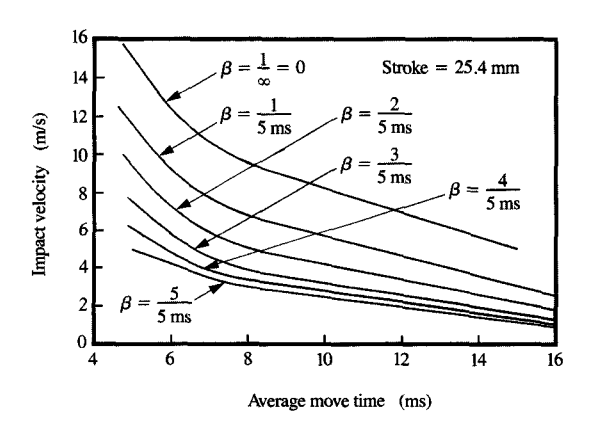
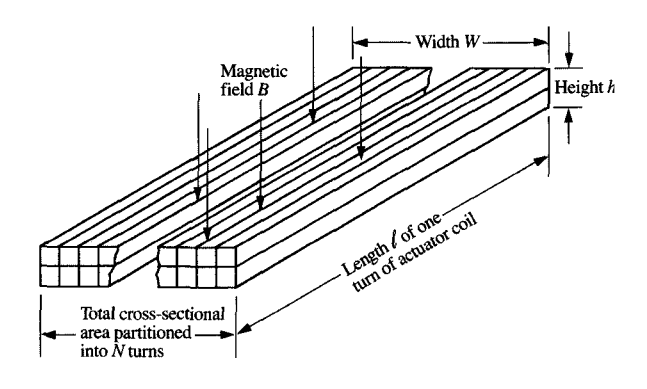


Figure 10

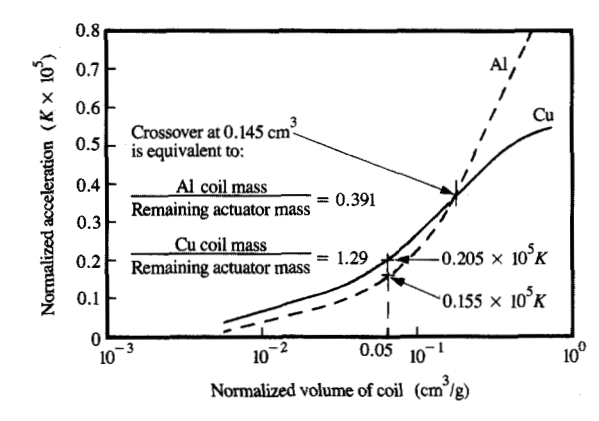
Calculated impact velocity versus average move time, at different values of mechanical time constant $1/\beta$.



Rigure 11

Actuator coil as a current sheet partitioned into n turns.

It follows that β can be increased with greater flux density, the immersion of the entire coil in its magnetic flux, use of a large coil mass relative to remaining actuator mass, and use of a high-conductivity coil material. Similarly, it follows that the actuator acceleration constant α can be maximized with use of high-conductivity wire, large flux density, the immersion of the entire coil in its magnetic flux, the use of a large coil mass relative to the remaining actuator mass, the use of a greater sheet width for an equal current sheet volume, and the partitioning of the coil volume into fewer turns.



Normalized acceleration versus normalized volume of coil, for unit actuator mass.

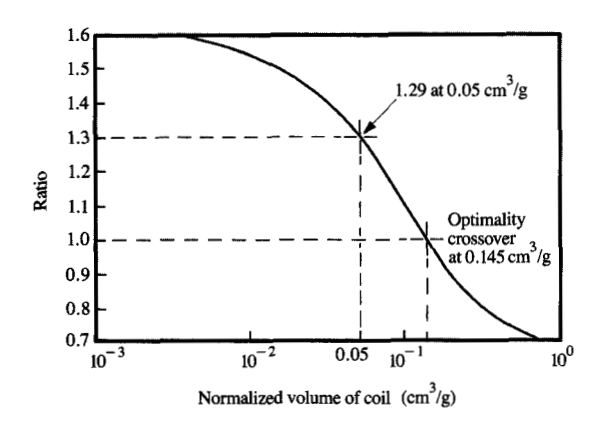


Figure 13

Ratio of the two curves of Figure 12 versus volume of coil.

Copper is the material commonly used for the formed current sheet, but occasionally aluminum is advantageous when current sheet mass, $M_{\rm c}$, approaches remaining actuator mass, $M_{\rm a}$. The use of aluminum, whose density and resistivity are 0.304 and 1.6 that of copper, respectively, facilitates a reduced mass but increased coil resistance. It is of interest, therefore, to determine for what ratio of sheet mass to actuator mass the use of aluminum becomes beneficial.

Spatial design constraints usually exist with respect to sheet volume, however, and not to sheet mass. The crossover from optimality with copper to that using aluminum is found by plotting a normalized version of Equation (15) or (16) as a function of coil volume

$$\alpha = \frac{\sigma V}{DV + M_0} K_1, \tag{17}$$

$$\beta = \frac{\sigma V}{DV + M_a} K_2, \tag{18}$$

where
$$K_1 = \frac{\gamma B}{\ell N}$$
,

and $K_2 = \gamma^2 B^2$. A common expression in terms of remaining actuator mass and coil volume, density, and conductivity results. If the common expression is plotted as shown in **Figure 12** with M_a as a one-gram unit mass, it is seen that the use of aluminum becomes beneficial beyond a sheet volume to remaining actuator mass ratio of 0.145 cm³/g. The equivalent aluminum and copper coil masses are, respectively, 0.391 and 1.29 grams, and the ratios of coil mass to remaining actuator mass are, respectively, 0.391 and 1.29. Unlike the power optimal consideration [1], Figure 12 shows no global extrema as a function of coil volume. Acceleration and mechanical time constant reciprocal are increasingly maximized with increased coil volume.

The ratio of the two curves of Figure 12 is plotted in Figure 13 and may be used to assess the optimality of actuator designs. The plots of Figures 12 and 13 are normalized with respect to a unit actuator mass of one gram. For other actuator masses, the horizontal scales are directly proportional to the ratio of actuator mass to its normalized value of one gram, and the vertical scales are unchanged. A remaining actuator mass M_a of 100 grams, for example, with 5 cm³ aluminum coil volume would have a normalized acceleration constant and normalized reciprocal mechanical time constant of $0.155K \times 10^5$. The curves of Figures 12 and 13 indicate that substitution of copper as the coil material should yield a 29% improvement in acceleration constant α and reciprocal mechanical time constant β .

A design strategy for minimum crash-stop impact velocity would therefore be to maximize magnetic flux density, use copper wire for all but very large coil volumes, use a coil mass that dominates the actuator-less-coil mass, and use a coil with very few turns. Note that this design strategy closely parallels that of minimum-power design [1], which similarly argues for large flux density, aluminum wire, and fewer turns. For optimal power design, however, optimal coil mass equals actuator-less-coil mass, and there is a trade-off between

coil height and magnetic flux density. Product coil designs rarely, if ever, achieve coil-mass optimality.

Interestingly, there is a region of normalized coil volume to actuator mass ratio whose choice of coil material depends upon which constraint to improved access time—air-bearing compliance or coil-power dissipation—is active. Copper is the correct coil material for all nominalized coil volumes less than 0.05 cm³/g. Between 0.05 cm³/g and 0.145 cm³/g, however, the superior choice of coil material is aluminum if coil-power dissipation limits move time. Conversely, if air-bearing compliance limits move time, copper is preferred. Beyond a coil volume of 0.145 cm³/g, aluminum is the proper coil material for either constraint.

• Rotary actuator

The current sheet may be incorporated into a rotary actuator, as shown schematically in Figure 14. The current sheet is considered as a point mass M_c at radius r_1 from the pivot, and the remaining actuator mass, exclusive of the coil, is a point mass M_a at radius r_2 . The position transducer is located at radius r_3 from the pivot and moves through an angular displacement x_1 . Since $K_t = K_f r_1$, and using K_f from Equation (12), α and β from Equation (11) become

$$\alpha = \frac{K_{\rm t}}{JR_{\rm coil}} = \frac{\gamma r_{\rm 1}B\ell N}{\left(M_{\rm c}r_{\rm i}^2 + M_{\rm a}r_{\rm 2}^2\right)\frac{\ell^2N^2}{\sigma V}}$$

$$=\frac{\sigma V \gamma B}{\left(DV + M_a \frac{r_2^2}{r_1^2}\right) r_1 \ell N},\tag{19}$$

$$\beta = \frac{K_{t}^{2}}{JR_{coil}} = \frac{\gamma^{2}r_{1}^{2}B^{2}\ell^{2}N^{2}}{\left(M_{c}r_{1}^{2} + M_{a}r_{2}^{2}\right)\frac{\ell^{2}N^{2}}{\sigma V}}$$

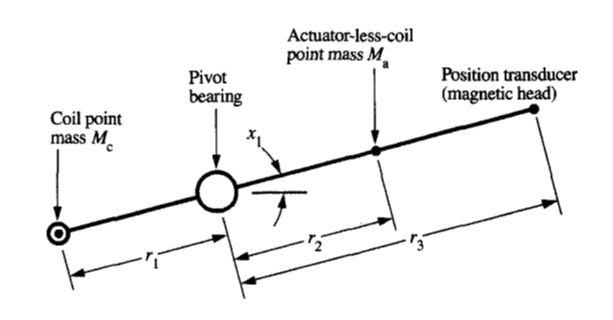
$$= \frac{\sigma V \gamma^2 B^2}{\left(DV + M_a \frac{r_2^2}{r_1^2}\right) r_1}.$$
 (20)

By differentiating α with respect to radius r_1 , a single global maximum for α exists when

$$r_1 = r_2 \sqrt{\frac{M_a}{M_a}},\tag{21}$$

which coincides with minimum power design [1]. On the other hand, β increases monotonically as radius r_1 becomes larger.

The design strategy for minimum crash-stop impact velocity is to maximize the mechanical time constant reciprocal to achieve, in the limit, identical velocity for



Flaure 14

Point mass schematic of rotary actuator with its current sheet.

all seek lengths, and to subsequently adjust the applied coil voltage for desired access performance. For the rotary actuator, therefore, a design objective is to make $M_c r_1^2$ approach if not exceed $M_a r_2^2$. In the limit, as $M_c r_1^2 \gg M_a r_2^2$, α and β become

$$\alpha = \frac{\sigma \gamma^2 B^2}{Dr},\tag{22}$$

$$\beta = \frac{B^2 \sigma}{D},\tag{23}$$

so that applied coil voltage must be increased proportionately to increases in r_1 for identical acceleration and move times.

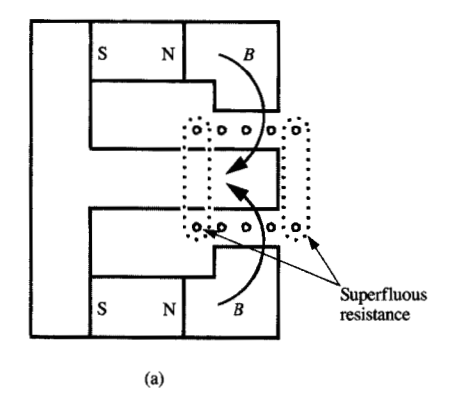
Note that optimum power design requires $M_c r_1^2 = M_a r_2^2$. If $M_c r_1^2 > M_a r_2^2$, improvements in minimizing crash-stop impact velocity are obtained at the expense of actuator power dissipation. The design choice of equality or of making $M_c r_1^2 > M_a r_2^2$ consequently derives from demonstrating which constraint, whether power or air-bearing compliance, limits actuator performance. If $M_c r_1^2 < M_a r_2^2$, improvements in meeting both constraints are made by increasing coil mass M_c and coil radius r_1 .

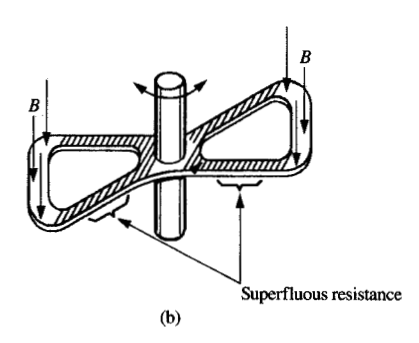
As in the case of the linear actuator, there is an optimal choice of coil material that minimizes crash-stop impact velocity. If Equations (19) and (20) are normalized as

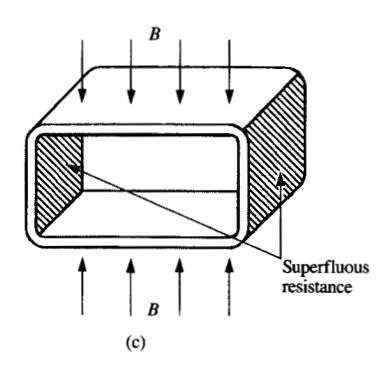
$$\alpha = \frac{\sigma V}{DV + \frac{r_2^2}{r_1^2} M_a} \tag{24}$$

where
$$K_1 = \frac{\gamma B}{r_1 \ell N}$$
, or

677







Inefficient coil designs with superfluous resistance: (a) long coilshort gap; (b) butterfly coil; (c) picture frame coil. The designs produce an increased impact velocity for a prescribed access-time performance.

$$\beta = \frac{\sigma V}{DV + \frac{r_2^2}{r_1^2} M_{\rm a}} K_2,$$
 (25)

where
$$K_2 = \frac{\gamma^2 B^2}{r_1}$$
,

a common expression in terms of remaining actuator mass and coil pivot radius, volume, density, and conductivity results that is similar to that of the linear actuator case. The linear actuator optimality curves of Figures 12 and 13 may therefore be extended to those of the rotary if the linear actuator $M_{\rm a}$ of Figures 12 and 13 is replaced by

$$M_{\rm a}\frac{r_{\rm 2}^2}{r_{\rm 1}^2}.$$

All the arguments related to optimal linear coil mass and selection of coil material as a function of move-time constraints, whether air-bearing compliance or coil-power dissipation, now map to the rotary case.

Usually minimum form factor and packaging restrictions compel the selection of a rotary actuator for an HDA design. The same constraints require radius r_1 to be smaller than r_2 , with a resultant large suboptimal mechanical time constant derived from making the motor back emf small relative to the applied coil voltage. Neither rotary nor linear actuators, however, have an inherent advantage in confronting the air-bearing constraint. Nonetheless, the rotary may exploit its additional flexibility with the choice of radii r_1 and r_2 if equal HDA volume designs are compared.

For either rotary or linear actuators it is important to avoid motor designs that inadvertently insert a nonfunctional resistance in series with the active coil portion that develops acceleration/deceleration force. Figure 15 shows actuator coil designs that produce increased impact velocity for a prescribed access time. One such configuration is a long-coil/short-gap design, in which the portion of the coil external to the magnetic field provides superfluous resistance. Another is a picture frame coil, in which only two of the four frame sides provide force in the proper radial direction. A third is a "butterfly coil" commonly used on rotary actuators, in which coil center and end portions add nonfunctional coil resistance. Note that the extraneous resistance of the butterfly coil is not detrimental if the actuator is already compromised with a large mechanical time constant in which $r_2 > r_1$.

By contrast, the circular coil permits magnetic-field designs that symmetrically immerse the entire coil in magnetic flux. The circular coil has no unnecessary, nonfunctional resistance; all portions of the coil contribute to providing acceleration and deceleration forces. The bang-bang principle [12] for transporting an object to a target location in minimum time—by the use of maximum acceleration followed by maximum deceleration—favors the air-bearing compliance constraint, and thus also the use of the entirely immersed circular coil, as designed to produce a small mechanical time constant.

Summary

In order to extract improved performance from a disk file, all facets pertaining to the air-bearing compliance constraint should be optimized. This paper attempts to illuminate the effects of the air-bearing slider design, the crash-stop design, and the actuator design on this accesstime constraint. The use of large sliders of high density and smaller air-bearing preload force prevents the achievement of large crash-stop deceleration and should to be avoided. Improved crash stops approaching the optimal constant deceleration force design should permit up to a $\sqrt{2}$ increase in crash-stop impact velocity, and a $\sqrt{2}$ decrease in access time for a well-designed, fast time constant actuator. Alternatively, for identical impact velocities, product cost per gigabyte should be improved by reducing compression distance by half. Finally, it is inferred that identical move time, but with reduced crash-stop impact velocity, should be obtained with actuators having fast mechanical time constants. Rotary actuators are equivalent in performance to linear actuators, but hold a distinct disadvantage if packaging constraints result in the use of a geometry that is intrinsic to large mechanical time constants. A design strategy for both has been prescribed.

Acknowledgments

The author acknowledges discussions with Dave Albrecht and the helpful suggestions of Rudy Lissner, Kenneth Deckert, and H. H. Ottesen.

References

- E. S. Cooper, "Minimizing Power Dissipation in a Disk File Actuator," *IEEE Trans. Magnetics* 24, No. 3, 2081–2091 (1988).
- T. Kailath, *Linear Systems*, Prentice-Hall, Inc., Englewood Cliffs, NJ, 1980, pp. 187–258.
- 3. P. S. Maybeck, Stochastic Models, Estimation, and Control, Academic Press, Inc., New York, 1979, Vol. I, pp. 133–195, Vol. II, pp. 1–193.
- E. S. Cooper, "A Disk File Servo Mechanism Immunized to Media Defects," *IEEE Trans. Magnetics* MAG-21, No. 6, 2592–2594 (1985).
- R. K. Oswald, "The IBM 3370 Head-Positioning Control System," *IBM Disk Storage Technology*, pp. 41–44; Order No. GA026-1665; available through IBM branch offices.
- E. S. Cooper, "Design of a Reference-Velocity Generator," IEEE Trans. Magnetics MAG-21, No. 5, 2097–2103 (1985).
- R. C. Benson and F. E. Talke, "The Transition Between Sliding and Flying of a Magnetic Recording Slider," *IEEE Trans.* Magnetics MAG-23, No. 5, 3441-3443 (1987).
- D. B. Bogy and F. E. Talke, "Laser Doppler Interferometry on Magnetic Recording Systems," *IEEE Trans. Magnetics* MAG-21, No. 5, 1332-1337 (1985).
- G. L. Best, H. Sussner, D. E. Horne, and A. Chou, "Precise Optical Measurement of Slider Dynamics," *IEEE Trans.* Magnetics MAG-22, No. 5, 1017–1018 (1986).
- J. A. Wagner, "The Actuator in High-Performance Disk Drives: Design Rules for Minimum Access Time," *IEEE Trans. Magnetics* MAG-19, No. 5, 1686-1688 (1983).
- 11. M. Tokuyama, Y. Yamaguchi, Y. Takeuchi, and I. Shimizu, "Reducing Flying Height Degradation due to Track Access

- Acceleration Acting on a Magnetic Head Slider," *IEEE Trans. Magnetics* MAG-23, No. 5, 3470–3472 (1987).
- M. Athans and P. L. Falk, Optimal Control, McGraw-Hill Book Co., Inc., New York, 1966.

Received May 31, 1989; accepted for publication December 1 1989

Evert S. Cooper IBM General Products Division, 5600 Cottle Road, San Jose, California 95193. Mr. Cooper received a B.S. degree in electronic engineering from California State Polytechnic University, Pomona, in 1966, and an M.S. degree from Santa Clara University, Santa Clara, California, in 1971. He is currently a Ph.D. candidate at Santa Clara University. Since joining IBM in 1966, Mr. Cooper has worked in the area of magnetic recording, including work on the IBM 3370 and 3375 DASD disk file positioning servomechanisms. He is a member of the IEEE and is currently involved in work on the digital control of head/disk assemblies.